A&A 521, L22 (2010)
DOI: 10.1051/0004-6361/201015081

Astronomy & Astrophysics
Special feature

Herschel/HIFI: first science highlights

Letter to the Editor

Herschel spectral surveys of star-forming regions

Overview of the 555–636 GHz range⋆,⋆⋆

C. Ceccarelli[1,2,3], A. Bacmann[1,2,3], A. Boogert[4], E. Caux[5,6], C. Dominik[7,8], B. Lefloch[1], D. Lis[9], P. Schilke[10,11], F. van der Tak[12,13], P. Caselli[14,15], J. Cernicharo[16], C. Codella[17], C. Comito[10], A. Fuente[18], A. Baudry[2,3], T. Bell[9], M. Benedettini[14], E. A. Bergin[19], G. A. Blake[9], S. Bottinelli[5,6], S. Cabrit[20], A. Castets[1,2,3], A. Coutens[5,6], N. Crimier[1,16], K. Demyk[5,6], P. Encrenaz[20], E. Falgarone[20], M. Gerin[20], P. F. Goldsmith[21], F. Helmich[12], P. Hennebelle[20], T. Henning[22], E. Herbst[23], P. Hily-Blant[1], T. Jacq[2,3], C. Kahane[1], M. Kama[7], A. Klotz[5,6], W. Langer[21], S. Lord[4], A. Lorenzani[17], S. Maret[1], G. Melnick[24], D. Neufeld[25], B. Nisini[26], S. Pacheco[1], L. Pagani[20], B. Parise[10], J. Pearson[21], T. Phillips[9], M. Salez[20], P. Saraceno[14], K. Schuster[27], X. Tielens[28], M. H. D. van der Wiel[12,13], C. Vastel[5,6], S. Viti[29], V. Wakelam[2,3], A. Walters[5,6], F. Wyrowski[10], H. Yorke[21] R. Liseau[30], M. Olberg[12,30], R. Szczerba[31], A. O. Benz[32], and M. Melchior[33]
(Affiliations are available on page 5 of the online edition)

Received 29 May 2010 / Accepted 7 July 2010

ABSTRACT

High resolution line spectra of star-forming regions are mines of information: they provide unique clues to reconstruct the chemical, dynamical, and physical structure of the observed source. We present the first results from the *Herschel* key project "Chemical *HErschel* Surveys of Star forming regions", CHESS. We report and discuss observations towards five CHESS targets, one outflow shock spot and four protostars with luminosities bewteen 20 and 2×10^5 $L_\odot$: L1157-B1, IRAS 16293-2422, OMC2-FIR4, AFGL 2591, and NGC 6334I. The observations were obtained with the heterodyne spectrometer HIFI on board *Herschel*, with a spectral resolution of 1 MHz. They cover the frequency range 555−636 GHz, a range largely unexplored before the launch of the *Herschel* satellite. A comparison of the five spectra highlights spectacular differences in the five sources, for example in the density of methanol lines, or the presence/absence of lines from S-bearing molecules or deuterated species. We discuss how these differences can be attributed to the different star-forming mass or evolutionary status.

Key words. astrochemistry – stars: formation

1. Introduction

The study of the chemical composition of the dense regions of the interstellar medium (ISM) has evolved enormously in the past few decades. It initiated with the detection of simple diatomic molecules, and was developed by with pioneering searches for polyatomic molecules. Today it aims to fully understand the chemistry of the ISM, how it depends on the specific physical conditions and evolves with time, and the ultimate molecular complexity reached in space. For several reasons, understanding the gas chemical composition during the process of star formation is of particular interest. First, the very process is influenced by the gas chemical composition. Second, since the chemical composition is in turn influenced by the evolutionary status of the forming protostar, it is a powerful diagnostic of the protostar evolution. Notable examples are the hot cores and hot corinos, which are thought to mark an evolutionary stage of high and low mass protostars, respectively. Finally, understanding the chemical composition during the star formation process permits us to predict, if not observe, the ultimate molecular complexity achieved in space, a mandatory first step to any exogenic theory of life on Earth. The only way to study the gas chemical composition is observing the line spectra from the different molecules and atoms in the gas. We highlight that another important aspect of observing and studying lines is their diagnostic power in reconstructing the dynamical and physical structure of the gas. In summary, line spectra are extremely powerful diagnostic tools enabling studies of virtually all aspects of the star formation process. Depending on the molecule/atom and the physical conditions, lines are emitted in the radio to far-infrared, at densities and temperatures appropriate to star-forming regions. Light molecules, such as hydrides, have fundamental transitions in the sub-millimeter/far-infrared range (between about 500 and 2000 GHz), so that these are the preferred ranges for detecting and studying these species. Heavy molecules, such as CO, have fundamental lines in the radio to millimeter frequency range: the heavier the molecule the lower the frequency. However, the higher the density and temperature the higher the frequency of the emitted line, so that sub-millimeter/far-infrared/near-infrared are the most appropriate frequency ranges for detecting and studying warm and dense gas. While frequencies from radio to millimeter, and partially sub-millimeter and near-infrared, can be observed from ground-based telescopes, frequencies between about 500 and 15 000 GHz are almost completely blocked by the Earth atmosphere, with some exceptions in a few narrow frequency ranges. The *Herschel* satellite is the first telescope capable of studying the 500−5000 GHz range of frequencies systematically (Pilbratt et al. 2010) and HIFI is the

⋆ *Herschel* is an ESA space observatory with science instruments provided by European-led principal Investigator consortia and with important participation from NASA.

⋆⋆ Figures 2–4 and Tables 3, 4 (pages 6 to 8) are only available in electronic form at http://www.aanda.org

Table 1. Selected sources.

Source	RA(J2000)	Dec(J2000)	Time (hr)	Dist. (pc)	Lum. ($L_\odot$)	Source type	Date	rms (mK)
L1544	05h04m17.21s	+25d10m42.8s	10	120	–	"Cold" pre-stellar core	–	–
I16293E	16h32m28.62s	–24d29m02.7s	10	120	–	"Warm" pre-stellar core	–	–
L1157-B1	20h39m10.20s	+68d01m10.5s	33	220	–	outflow shock spot	2009, Aug. 1	7–17
IRAS 16293-2422	16h32m22.75s	–24d28m34.2s	50	120	21	Class 0 low mass protostar	2010, Mar. 2	~10
OMC2-FIR4	05h35m26.97s	–05d09m54.5s	42	440	1×10^3	Intermediate mass protostar	2010, Mar. 2	~10
AFGL 2591	20h29m24.90s	+40d11m21.0s	34	1000	2×10^4	High mass protostar	2010, Apr. 12	~20
NGC 6334I	17h20m53.32s	–35d46m58.5s	42	1700	2×10^5	High mass protostar	2010, Mar. 2	~10
W51e	19h23m43.88s	+14d30m28.8s	10	7000	2×10^6	High mass protostar	–	–

first high-resolution spectrometer ever that enables us to study the 480−1907 GHz spectral range using heterodyne techniques (de Graauw et al. 2010).

The key project "Chemical *HErschel* Surveys of Star forming regions" (CHESS), takes full advantage of the new opportunity offered by *Herschel*/HIFI and explores in a systematic way the frequency range between 480 and 1902 GHz in several star-forming regions. The goal of the project is to provide the first ever spectral census of this frequency range in a selected sample of sources covering the principal parameters and aspects of the star-formation process: mass of the forming star, its evolutionary status, and the interaction with the surroundings. The sample is formed by eight sources (Table 1) whose proprieties cover a wide parameter space. To study the dependence on the mass of the forming star, we selected five low-, intermediate-, and high-mass protostars, which cover five orders of magnitude in luminosity, from 20 to 2×10^6 $L_\odot$. To study the dependence on the evolutionary status, we included two pre-stellar cores, with different characteristics. Finally, the sample includes one molecular outflow shock, to cover the aspect of the influence of the forming star on its surroundings. Almost the entire 480−1902 GHz frequency range will be covered in all sources, with the exceptions of the pre-stellar cores, where only the 480−636 GHz band will be observed together with a small range around 1 THz (to detect the HD_2^+ $1_{11}-0_{00}$ line). IRAS 16293-2422 and L1157-B1 will also be observed in the 57−210 μm range with the *Herschel*/PACS spectrometer. Here we present a first analysis of the 555−636 GHz spectra of five CHESS sources, obtained during the first months of operations of HIFI, and discuss similarities and differences between the sources.

2. Observations and results

Early observations were obtained with HIFI towards five CHESS sources in the 555−636 GHz frequency range. The sources were observed during the performance verification phase I (L1157-B1) and the priority science program (IRAS 16293-2422, OMC2-FIR4, AFGL 2591, and NGC 6334I). The dates of the observations and the rms achieved for each source are reported in Table 1. The observations were obtained in double-sideband (DSB) using the wide band spectrometer (WBS) whose resolution is about 1.1 MHz. The HPBW at the observed frequencies is ~35″. The data were processed with the standard HIFI pipeline using release 2.8 of HIPE (*Herschel* interactive processing environment)[1]. Further processing of the level 2 products was needed to flag spurious local oscillator features, subtract baselines, and deconvolve the dual sidebands. This was done both in HIPE and using the GILDAS[2] software and subsequently the results were cross-checked. To convert the obtained antenna temperatures into main beam temperatures we used $B_{\rm eff} = 0.72$, $F_{\rm eff} = 0.96$ and the beam efficiency defined as $\eta_{\rm mb} = F_{\rm eff}/B_{\rm eff}$. For the line identifications we used the JPL[3] and CDMS[4] databases, as well as the package CASSIS[5].

Figure 1 shows the 555−636 GHz spectra of the five sources of Table 1. Figures 2−4 show spectra zooms. Tables 3 and 4 list the lines detected with signal-to-noise ratio (SNR) greater than 3 in at least a source other than NGC 6334I, their integrated intensity, and line widths (typically between 2 and 10 km s^{-1}). The detected species are listed in Table 2.

3. Source differences and similarities

3.1. Sources background

L1157-B1 is a bright and chemically rich shock spot of the powerful outflow emanating from the class 0 source L1157-mm, regarded as the archetype of the so-called chemically rich outflows (Bachiller et al. 2001). The spatial and kinematical structure of the bright blueshifted bow-shock B1 in the southern lobe has been modelled in great detail by various authors, making it the archetype of protostellar bowshocks in low-mass star-forming regions and the testbed of MHD shock models (Gusdorf et al. 2008). A detailed study of the HIFI 555−636 GHz observations is found in Lefloch et al. (2010) and Codella et al. (2010).

IRAS 16293-2422 is the prototype of class 0 sources for studies of chemistry in low mass protostars. It is in this source that the super-deuteration phenomenon (Ceccarelli et al. 1998) and the first hot corino (Cazaux et al. 2003) has been discovered. The large-scale structure of its envelope has been reconstructed by several authors (e.g., Crimier et al. 2010). A complete survey of the 3, 2, 1, and 0.8 mm bands accessible from the ground detected a rich spectrum containing several deuterated and complex organic molecules (Caux et al. 2010). Bacmann et al. (2010), and Vastel et al. (2010) report the analysis of ND and D_2O observations obtained with HIFI.

OMC2-FIR4 is the closest known intermediate mass protostar. Its ~30 $M_\odot$ envelope extends to about 10^4 AU (Crimier et al. 2009) and contains several clumps, probably a cluster of protostars (Shimajiri et al. 2008). Previous observations show that the envelope has abundant formaldehyde (Jørgensen et al. 2006). The methanol emission observed with HIFI is discussed by Kama et al. (2010).

AFGL 2591 is a relatively nearby and isolated massive star, with a well-studied temperature and density structure (Van der Tak et al. 1999). Multi-line observations of CH_3OH, SO_2, and other molecules have revealed enhanced abundances in the inner envelope, where ice mantles are evaporating off dust grains (Van der Tak et al. 2000, 2003). On even smaller scales, interferometry of the $H_2^{18}O$ line at 203 GHz shows a rotating flattened

[1] HIPE is a joint development by the *Herschel* Science Ground Segment Consortium, consisting of ESA, the NASA *Herschel* Science Center, and the HIFI, PACS and SPIRE consortia.

[2] http://www.iram.fr/IRAMFR/GILDAS

[3] http://spec.jpl.nasa.gov; Pickett et al. 1998.

[4] http://cdms.de; Müller et al. 2005.

[5] http://cassis.cesr.fr/

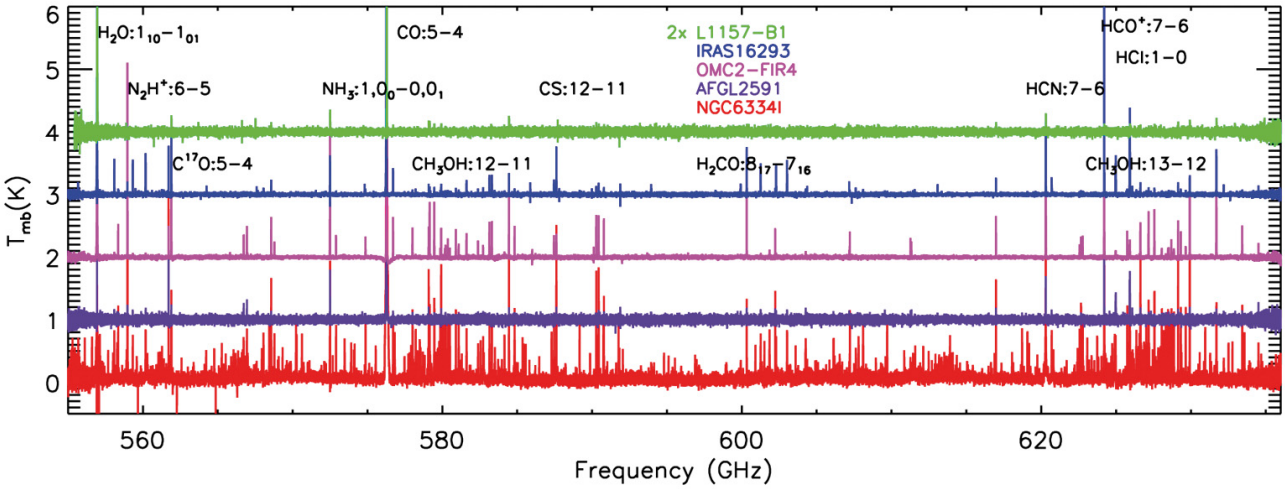

Fig. 1. Observed spectra (T_{mb}) in the 555−636 GHz range. The transitions of the brightest lines are marked. *From bottom to top*: NGC 6334I (red), AFGL 2591 (purple), OMC2-FIR4 (magenta), IRAS 16293-2422 (blue), and L1157-B1 (green). Note: the intensity is multiplied by 2 in L1157-B1.

structure, possibly a massive accretion disk (Van der Tak et al. 2006).

NGC 6334I is a relatively nearby molecular cloud/H II region complex containing several concentrations of massive stars at various stages of evolution. The far-infrared source "I" is associated with a NIR cluster (Sandell et al. 2000) with four embedded compact millimeter continuum sources (Hunter et al. 2006). Spectral survey data of McCutcheon et al. (2000) show a molecular environment rich in methanol, methyl formate, and dimethyl ether, with lines ranging in energy up to 900 K above the ground state. Lis et al. (2010), Emprechtinger et al. (2010), and van der Wiel et al. (2010) report the studies of the H_2Cl^+, H_2O, and CH lines.

3.2. Line spectra

The vast majority of the detected lines have upper level energies higher than ∼80 K (Table 2) and are, therefore, emitted in the warm (≥50 K) regions of the sources: hot cores, hot corinos, and shocked gas. A few lines (from H_2O, NH_3, HCl, and D_2O) have lower upper level energies and may, therefore, originate in cold gas. A rigorous comparison between the sources in terms of species abundance requires a detailed analysis that takes into account the structure of the sources, i.e., extent, density, and temperature ... – and their distance. Here we limit the discussion to the mere appearance of the spectra and postpone a more detailed study to a forthcoming article. Nonetheless, even qualitative comparison of the spectra provides new insights on the nature of the sources.

Overall, NGC 6334I exhibits the richest (in number of lines) and brightest spectrum, with more than 500 lines. IRAS 16293-2422 and OMC2-FIR4 have a smaller number of lines, ∼70, followed by AFGL 2591 and L1157-B1, ≤30. The spectra are dominated in terms of number by the methanol (CH_3OH) lines. In the case of NGC 6334, they constitute more than 70% of the detected lines. When considering the number of detected species, NGC 6334I and IRAS 16293-2422 share the first place with 26 and 22 detected species, followed by OMC2-FIR4, AFGL 2591, and L1157-B1 with 17, 11 and 8 detected species, respectively. We therefore note that the number of lines in a spectrum is not a unique criterium for its chemical richness. In the following, we discuss the more important differences between the sources in the spectra of the different species.

i) Methanol (CH_3OH). Several previous studies have established that methanol is sublimated or sputtered from the ices when the dust temperature exceeds about 100 K or the shock velocity is larger than about 20 km s^{-1}, rather than formed in the gas phase. The plethora of methanol lines with upper level energies up to 1000 K in NGC 6334I testifies that very hot material exists in its hot core. The lines there could be excited either by the collisions from the warm and dense gas or may be radiatively pumped by the hot dust, by means of "fluorescence" from the 2.7−97 μm photon-pumped CH_3OH vibrational levels. The same applies to IRAS 16293-2422 and OMC2-FIR4. In L1157-B1, the lines must be populated by collisions, which may explain why their number is smaller. It is striking how poor in methanol lines the spectrum of AFGL 2591 is, especially compared to IRAS 16293-2422 and OMC2-FIR4, which are much less luminous than AFGL 2591. Previously estimated methanol abundance in the warm envelope, 8×10^{-8}, and emitting sizes, ∼3″, (van der Tak et al. 2000) are comparable to those measured in IRAS 16293-2422 (Maret et al. 2005), so that the weaker methanol lines in AFGL 2591 may be indicative of lower interior densities or gas temperatures.

ii) Sulphur bearing molecules. The detected lines of CS, H_2S, SO, and SO_2 have all relatively high upper level energies (≥80 K: Table 2) so that they must originate in warm and dense gas. As for methanol, sulphur is mostly released from the ices in hot cores, hot corinos, and outflow shocks. A remarkable result of the 555−636 GHz spectra comparison is the lack of emission from S-bearing molecules in OMC2-FIR4, with the exception of CS, and of H_2S and SO_2 in AFGL 2591. Several authors have demonstrated how the relative abundances of H_2S, SO, and SO_2 are influenced by the differences in the (sublimated) ice composition, the age of the source, or the gas temperature. In general, the overabundance of SO with respect to SO_2 points towards a younger source (e.g. Wakelam et al. 2005), so that AFGL 2591 may be a very young massive protostar (see also van der Tak et al. 2003). In contrast, the absence of H_2S, SO, and SO_2 in OMC2-FIR4 is puzzling, because sublimated ices are clearly indicated by the presence of several and bright methanol lines. One possibility is that while the dust is warm enough to sublimate the ices, the gas temperature is not high enough to activate the reactions to convert whatever is sublimated from the ices and that it is not H_2S: it could be OCS or atomic sulphur (e.g. Wakelam et al. 2005) into H_2S, SO, and SO_2. This would be consistent with a theoretical study by Crimier et al. (2009), who predicts an inner region where the gas is much cooler than the dust because of the efficient cooling by the water molecules. This

Table 2. Species and number of detected lines in the 555−636 GHz.

Species	E_{up} (K)	(1)	(2)	(3)	(4)	(5)
H_2O	27–680	1	2	1	1	2
HDO	97	0	1	0	0	1
D_2O	29	0	1	0	0	0
CO	83	1	1	1	1	1
$C^{17}O$	83	0	1	1	1	1
HCO^+	119	1	1	1	1	1
$H^{13}CO^+$	119	0	1	0	0	1
HCN	119	1	1	1	1	1
$H^{13}CN$	119	0	1	1	0	1
DCN	119	0	1	0	0	1
HNC	119	0	1	1	0	1
CN	82	0	0	2	2	2
N_2H^+	95	0	1	1	0	1
NH_3	28	1	1	1	1	1
HCl	27	0	1	1	1	1
$H^{37}Cl$	27	0	1	1	0	1
CCH	117	0	0	2	0	2
H_2CO	120–530	4	8	8	0	8
CH_3OH	39–1050	17	35	47	3	345
$^{13}CH_3OH$	39–240	0	0	0	0	41
CH_3OCH_3	115–290	0	0	1	0	30
H_2S	160–415	0	2	0	0	4
CS	186	1	1	1	1	1
$C^{34}S$	175–200	0	2	0	0	2
SO	190–225	0	6	0	2	6
SO_2	80–210	0	10	0	0	15
others[c]		0	0	0	0	62
Total		27	86	71	16	558

Notes. Second column gives the upper level energy range of the detected transitions. Columns (1) to (5) refer to L1157-B1, IRAS 16293, OMC2-FIR4, AFGL 2591 and NGC 6334I respectively. In L1157-B1 the number refers to the list of lines reported in Codella et al. (2010).

hypothesis needs further studies for confirmation. Observations of the S line at 56 μm with *Herschel*/PACS will certainly help us to solve the puzzle.

iii) Deuterated molecules. Singly deuterated species (HDO and DCN) are only detected in IRAS 16293-2422 and NGC 6334I, while a doubly deuterated species, D_2O, is only detected in IRAS 16293-2422. Given the upper level energies of the detected transitions of the singly deuterated species (Table 2), they reside in the hot core and hot corino of NGC 6334I and IRAS 16293-2422, respectively. While DCN is most likely a gas phase product, HDO is sublimated from the dust ices and, therefore, reflects the prior history of the protostar. In contrast, the ortho-D_2O fundamental transition is observed in absorption in IRAS 16293-2422 (Vastel et al. 2010). In this case, the cold gas in the envelope is responsible for the large ortho-D_2O abundance. The detection of D_2O in IRAS 16293-2422 and not in the other sources, does not come as a total surprise, as IRAS 16293-2422 is known to be a source enriched by singly, doubly, and triply deuterated molecules (e.g., Parise et al. 2006). However, the present observations indicate that intermediate and high mass protostars (at least those targeted here) are much less enriched in D-bearing molecules, probably because of the higher temperature and gaseous CO abundance in these protostars (Roberts et al. 2003).

4. Conclusions

Our comparative analysis of the 555–636 GHz spectra in five CHESS sources has discovered an unexpected line-poor spectrum in the 2×10^4 $L_\odot$ source AFGL 2591. This may indicate that AFGL 2591 is a particularly young protostar that has not had time to develop a rich chemistry. Our analysis also confirms IRAS 16293-2422 as a remarkable source of enriched deuterated molecules and NGC 6334I as being enriched in methanol lines. OMC2-FIR4 seems to represent a bridge between the two extremes in luminosity, represented by IRAS 16293-2422 and NGC 6334I, but is not a scaled version of either of the two sources. It shares the richness, even though more moderately, in methanol lines with NGC 6334I but shows a desert in S-bearing molecules, maybe because of a dramatic decoupling of gas and dust temperatures in the interior of its envelope. Finally, the outflow shock, is affected by the same lack of S-bearing molecules, but this, as for the relative line-poor spectrum in general, could simply be due to the sensitivity of the current observations.

To conclude, we highlight again the power of unbiased surveys of the spectral range accessible to HIFI (480−1902 GHz). In this short time of operation, the survey data have permitted the detection of several new molecules (H_2O^+ by Ossenkopf et al. 2010; OH^+ by Gerin et al. 2010; H_2Cl^+ by Lis et al. 2010, ortho-D_2O by Vastel et al. 2010; and ND by Bacmann et al. 2010). They also permit an overall comparative study that is far more exhaustive than targeted studies of individual sources.

Acknowledgements. HIFI has been designed and built by a consortium of institutes and university departments from across Europe, Canada and the United States under the leadership of SRON Netherlands Institute for Space Research, Groningen, The Netherlands and with major contributions from Germany, France abd the US. Consortium members are: Canada: CSA, U. Waterloo; France: CESR, LAB, LERMA, IRAM; Germany: KOSMA, MPIfR, MPS; Ireland, NUI Maynooth; Italy: ASI, IFSI-INAF, Osservatorio Astrofisico di Arcetri-INAF; Netherlands: SRON, TUD; Poland: CAMK, CBK; Spain: Observatorio Astronómico Nacional (IGN), Centro de Astrobiología (CSIC-INTA). Sweden: Chalmers University of Technology – MC2, RSS & GARD; Onsala Space Observatory; Swedish National Space Board, Stockholm University – Stockholm Observatory; Switzerland: ETH Zurich, FHNW; USA: Caltech, JPL, NHSC. We thank many funding agencies for financial support.

References

Bachiller, R., Peréz-Gutierrez, M., Beltrán, M., et al. 2001, A&A, 372, 899
Bacmann, A., Caux, P., Hily-Blant, B., et al. 2010, A&A, 521, L42
Cazaux, S., Tielens, X., Ceccarelli, C., et al. 2003, ApJ, 593, L51
Caux, E., Kahane, C., Castets, A., et al. 2010, A&A, submitted
Ceccarelli, C., Castets, A., Loinard, L., et al. 1998, A&A, 338, L43
Codella, C., Lefloch, B., Ceccarelli, C., et al. 2010, A&A, 518, L112
Crimier, N., Ceccarelli, C., Lefloch, B., et al. 2009, A&A, 506, 1229
Crimier, N., Ceccarelli, C., Maret, S., et al. 2010, A&A, 519, A65
de Graauw, Th., Helmich, F. P, Phillips, T. G, et al. 2010, A&A, 518, L6
Emprechtinger, M., Lis, D. C., Bell, T., et al. 2010, A&A, 521, L28
Gerin, M., De Luca, M., Black, J., et al. 2010, A&A, 518, L110
Gusdorf, A., Pineau des Forets, G., Cabrit, S., et al. 2008, A&A, 490, 695
Hunter, T. R., Brogan, C. L., Megeath, S. T., et al. 2006, ApJ, 649, 888
Kama, M., Dominik, C., Maret, S., et al. 2010, A&A, 521, L39
Lefloch, B., Cabrit, S., Codella, C., et al. 2010, A&A, 518, L113
Lis, D. C., Pearson, J. C., Neufeld, D. A., et al. 2010, A&A, 521, L9
Jørgensen, J., Johnstone, D., van Dishoeck, E., et al. 2006, A&A, 206, 449
Maret, S., Ceccarelli, C., Tielens, X., et al. 2005, A&A, 442, 527
McCutcheon, W. H., Sandell, G., Matthews, H. E., et al. 2000, MNRAS, 316, 152
Ossenkopf, V., Müller, H., Lis, D., et al. 2010, A&A, 518, L111
Parise, B., Ceccarelli, C., Tielens, X., et al. 2006, A&A, 453, 949
Pickett, H. M., Poynter, I. R. L., Cohen, E. A., et al. 1998, JQSRT, 60, 883
Pilbrat, G. L., Riedinger, J. R., Passvogel, T., et al. 2010, A&A, 518, L1
Roberts, H., Millar, T., & Herbst, E. 2003, ApJ, 591, L41
Sandell, G. 2000, A&A, 358, 242
Shimajiri, Y., Takahashi, S., Takakuwa, S., et al. 2008, ApJ, 683, 255
van der Tak, F., van Diishoeck, E., Evans, N. J., et al. 1999, ApJ, 522, 1010
van der Tak, F., van Diishoeck, E., & Caselli, P. 2000, ApJ, 361, 327
van der Tak, F., Boonman, A., Braakman, R., et al. 2003, A&A, 412, 133
van der Tak, F., Wasmley, M., Herpin, F., et al. 2006, A&A, 447, 1011
van der Wiel, M. H. D., van der Tak, F., Lis, D. C., et al. 2010, A&A, 521, L43
Vastel, C., Ceccarelli, C., Caux, E., et al. 2010, A&A, 521, L31
Wakelam, V., Caselli, P., Ceccarelli, C., et al. 2004, A&A, 422, 159
Zhang, Q., & Ho, P. T. P. 1997, ApJ, 488, 241

[1] Laboratoire d'Astrophysique de Grenoble, UMR 5571-CNRS, Université Joseph Fourier, Grenoble, France
e-mail: cecilia.ceccarelli@obs.ujf-grenoble.fr
[2] Université de Bordeaux, Laboratoire d'Astrophysique de Bordeaux, Floirac, France
[3] CNRS/INSU, UMR 5804, Floirac Cedex, France
[4] Infared Processing and Analysis Center, Caltech, Pasadena, USA
[5] Centre d'Etude Spatiale des Rayonnements, Université Paul Sabatier, Toulouse, France
[6] CNRS/INSU, UMR 5187, Toulouse, France
[7] Astronomical Institute "Anton Pannekoek", University of Amsterdam, Amsterdam, The Netherlands
[8] Department of Astrophysics/IMAPP, Radboud University Nijmegen, Nijmegen, The Netherlands
[9] California Institute of Technology, Pasadena, USA
[10] Max-Planck-Institut für Radioastronomie, Bonn, Germany
[11] Physikalisches Institut, Universität zu Köln, Köln, Germany
[12] SRON Netherlands Institute for Space Research, Groningen, The Netherlands
[13] Kapteyn Astronomical Institute, University of Groningen, The Netherlands
[14] INAF - Istituto di Fisica dello Spazio Interplanetario, Roma, Italy
[15] School of Physics and Astronomy, University of Leeds, Leeds, UK
[16] Centro de Astrobiologìa, CSIC-INTA, Madrid, Spain
[17] INAF Osservatorio Astrofisico di Arcetri, Florence Italy
[18] IGN Observatorio Astronómico Nacional, Alcalá de Henares, Spain
[19] Department of Astronomy, University of Michigan, Ann Arbor, USA
[20] Laboratoire d'Études du Rayonnement et de la Matière en Astrophysique, UMR 8112 CNRS/INSU, OP, ENS, UPMC, UCP, Paris, France
[21] Jet Propulsion Laboratory, Caltech, Pasadena, CA 91109, USA
[22] Max-Planck-Institut für Astronomie, Heidelberg, Germany
[23] Ohio State University, Columbus, OH, USA
[24] Harvard-Smithsonian Center for Astrophysics, Cambridge MA, USA
[25] Johns Hopkins University, Baltimore MD, USA
[26] INAF - Osservatorio Astronomico di Roma, Monte Porzio Catone, Italy
[27] Institut de RadioAstronomie Millimétrique, Grenoble, France
[28] Leiden Observatory, Leiden University, Leiden, The Netherlands
[29] Department of Physics and Astronomy, University College London, London, UK
[30] Chalmers University of Technology, Department of Astronomy, Stockholm University, Stockholm, Sweden
[31] N. Copernicus Astronomical Center, Torun, Poland
[32] Institute of Astronomy, ETH Zurich, 8093 Zurich, Switzerland
[33] Institut für 4D-Technologien, Switzerland

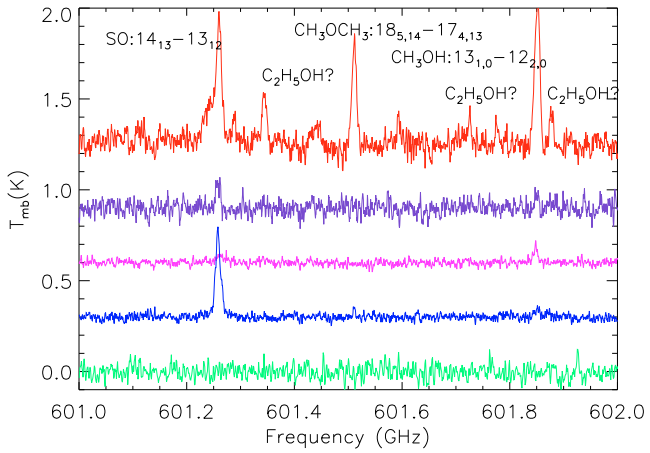

Fig. 2. Zoom around the SO line $14_{13}-13_{12}$ at 601.258 GHz. The other lines in the spectrum are from CH_3OH, CH_3OCH_3 as marked. Thre weaker lines are likely from ethanol (C_2H_5OH. Colours are as in Fig. 1. From bottom to top: L1157-B1, IRAS 16293-2422, OMC2-FIR4, AFGL 2591, and NGC 6334I.

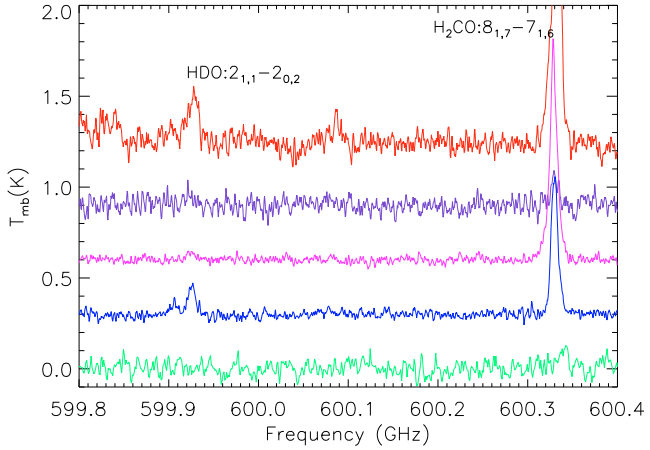

Fig. 3. Zoom around the HDO line $2_{1,1}-2_{0,2}$ at 599.927 GHz and the H_2CO line $8_{1,7}-7_{1,6}$ at 600.331 GHz. Colours are as in Fig. 1. From bottom to top: L1157-B1, IRAS 16293-2422, OMC2-FIR4, AFGL 2591, and NGC 6334I.

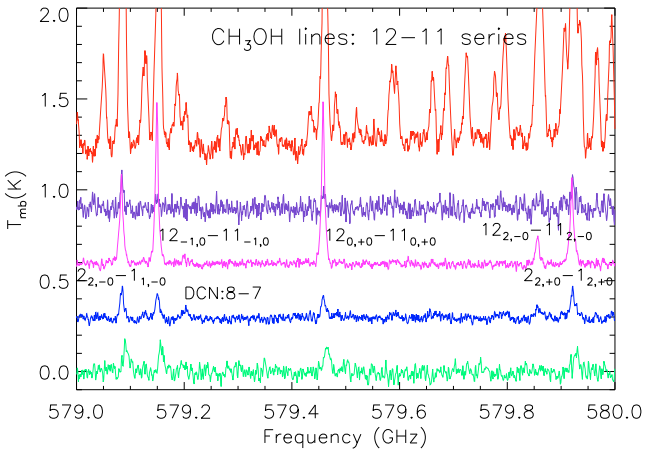

Fig. 4. Zoom around the CH_3OH lines of the 12-11 series. The transitions of the brightest lines are marked following the JPL catalog. The DNC 8-7 line lies at 579.205 GHz. Colours are as in Fig. 1. From bottom to top: L1157-B1, IRAS 16293-2422, OMC2-FIR4, AFGL 2591, and NGC 6334I.

Table 3. List of detected lines, for all species except CH_3OH and CH_3OCH_3.

Transition	Freq.	L1157-B1		IRAS 16293		OMC2-IRAS 4		AFGL 2591		NGC 6334I	
		$T_{\rm mb}\Delta v$	Δv	$T_{\rm mb}\Delta v$	Δv	$T_{\rm mb}\Delta v$	Δv	$T_{\rm mb}\Delta v$	Δv	$T_{\rm mb}\Delta v$	Δv
	(GHz)	K km s^{-1}	km s^{-1}	K km s^{-1}	km s^{-1}	K km s^{-1}	km s^{-1}	K km s^{-1}	km s^{-1}	K km s^{-1}	km s^{-1}
H_2O: $1_{10}-1_{01}$	556.936	14.75(0.33)	11.6	17.62(0.49)	6.8	17.26(0.57)	8.8	3.35(0.46)	3.0	≤1.51[a]	–
H_2O: $5_{32}-4_{41}$	620.701	≤0.12	–	1.80(0.18)	9.9	≤0.15	–	≤0.43	–	5.15(0.52)[a]	8.8
HDO: $2_{11}-2_{02}$	599.927	≤0.12	–	0.73(0.23)	4.6	≤0.11	–	≤0.35	–	1.67(0.45)	6.8
CO: 5–4	576.268	54.20(0.32)	4.8	87.78(1.82)	9.7	147.59(0.74)	11.3	165.52(0.93)	7.8	133.63(9.63)[a]	4.2
$C^{17}O$: 5–4	561.713	≤0.16	–	2.46(0.32)	2.9	1.09(0.17)	2.2	4.28(0.57)	3.4	15.47(0.89)	4.6
HCO^+: 7–6	624.208	0.11(0.03)	–	17.70(0.18)	2.4	16.87(0.18)	4.1	9.99(0.40)	3.8	32.36(1.24)	5.9
$H^{13}CO^+$: 7–6	607.175	≤0.12	–	0.68(0.24)	3.0	≤0.96	–	≤0.37	–	4.12(3.60)	5.0
HCN: 7–6	620.304	0.96(0.13)	7.4	5.45(0.16)	5.2	16.87(0.38)	8.9	2.66(0.28)	3.7	21.39(0.70)	8.0
$H^{13}CN$: 7–6	604.268	≤0.10	–	0.57(0.14)	6.0	0.77(0.11)	12.3	≤0.33	–	6.81(0.43)[b]	12.9
DCN: 8–7	579.205	≤0.09	–	0.29(0.12)	6.0	≤0.10	2.5 –	≤0.28	–	1.2(4.38)[b]	4.2
HNC: 7–6	634.510	≤0.18	–	0.58(0.17)	3.8	0.35(0.20)	1.7	≤0.45	–	3.26(0.74)	6.6
CN: $5_{05}-4_{04}$	566.731	≤0.09	–	≤0.09	–	1.77(0.10)	6.1	0.79(0.25)	3.2	4.13(1.49)	7.8
CN: $5_{06}-4_{05}$	566.947	≤0.11	–	≤0.10	–	1.39(0.19)	3.4	0.98(0.26)	3.0	4.12(1.38)	5.8
N_2H^+: 6–5	558.967	≤0.14	–	0.45(0.15)	1.9	6.84(0.12)	2.2	≤0.26	–	11.87(1.77)	4.5
NH_3: $1, 0_0-0, 0_1$	572.497	1.26(0.09)	7.6	2.8(0.15)[b]	3.5	8.32(0.14)	4.5	3.52(0.27)	4.2	7.79(0.66)	3.8
HCl[c] : 1–0	625.902	≤0.13	–	2.24(0.15)	2.0	0.42(0.14)	2.2	2.05(0.30)	3.1	20.06(1.34)[b]	18.5
$H^{37}Cl$[c] :1–0	624.978	≤0.13	–	0.76(0.18)	1.5	0.28(0.12)	4.1	≤0.33	–	5.63(3.09)	13.4
CCH: 7_8-6_7	611.265	≤0.11	–	≤0.11	–	0.78(0.13)	2.8	≤0.26	–	2.15(1.06)	7.2
CCH: 7_7-6_6	611.328	≤0.11	–	≤0.12	–	0.84(0.15)	3.9	≤0.26	–	1.33(1.15)	6.1
H_2CO: $8_{18}-7_{17}$	561.899	0.63(0.11)	4.4	4.21(0.18)	4.2	6.61(0.16)	4.3	≤0.39	–	9.98(0.59)	6.5
H_2CO: $8_{08}-7_{07}$	576.708	0.39(0.11)	7.9	2.00(0.10)	4.5	2.65(0.10)	4.2	≤0.22	–	7.13(0.48)	7.1
H_2CO: $8_{27}-7_{26}$	581.612	≤0.09	–	1.19(0.11)	5.2	1.53(0.12)	4.1	≤0.26	–	4.40(0.52)	5.3
H_2CO: $8_{54}-7_{53}$	582.382	≤0.09	–	0.51(0.15)	6.2	0.79(0.14)	3.4	≤0.27	–	3.16(0.38)	5.7
H_2CO: $8_{35}-7_{34}$	583.309	≤0.11	–	1.57(0.14)	4.9	2.01(0.12)	3.9	≤0.32	–	5.39(0.83)	5.9
H_2CO: $8_{26}-7_{25}$	587.454	≤0.12	–	1.18(0.14)	4.9	1.18(0.12)	3.7	≤0.35	–	4.05(0.45)	4.8
H_2CO: $8_{17}-7_{16}$	600.331	0.19(0.04)	8.2	3.43(0.19)	4.3	5.11(0.14)	4.6	≤0.37	–	8.79(0.50)	6.7
H_2CO: $8_{19}-7_{18}$	631.703	0.44(0.11)	3.8	3.41(0.15)	4.4	5.08(0.14)	4.4	≤0.35	–	8.14(0.69)	6.4
H_2S: $6_{42}-6_{33}$	567.080	≤0.09	–	≤0.10	–	≤0.09	–	≤0.21	–	1.46(0.73)	9.2
H_2S: $3_{31}-3_{22}$	568.051	≤0.08	–	0.48(0.13)	4.5	≤0.14	–	≤0.22	–	3.40(0.50)	5.0
H_2S: $5_{50}-5_{41}$	579.795	≤0.09	–	≤0.13	–	≤0.14	–	≤0.23	–	2.84(0.50)	5.2
H_2S: $5_{32}-5_{23}$	611.442	≤0.10	–	0.40(0.14)	6.4	≤0.11	–	≤0.25	–	1.98(0.72)	6.4
CS: 12–11	587.616	0.19(0.03)	5.2	3.18(0.17)	4.2	4.10(0.14)	10.9	0.92(0.28)	4.5	15.13(0.49)	6.7
$C^{34}S$: 12–11	578.216	≤0.09	–	0.42(0.11)	5.4	≤0.11	–	≤0.24	–	8.68(0.50)	7.7
$C^{34}S$: 13–12	626.349	≤0.11	–	0.40(0.14)	5.0	≤0.15	–	≤0.31	–	3.92(0.69)	5.4
SO: $13_{12}-12_{11}$	558.087	≤0.14	–	2.77(0.14)	5.2	≤0.14	–	≤0.30	–	3.55(0.33)	4.9
SO: $13_{13}-12_{12}$	559.319	≤0.11	–	2.88(0.14)	5.4	≤0.12	–	≤0.33	–	3.64(0.35)	5.6
SO: $13_{14}-12_{13}$	560.178	≤0.11	–	3.12(0.17)	5.1	≤0.12	–	0.76(0.22)	4.4	4.83(0.37)	6.6
SO: $14_{13}-13_{12}$	601.258	≤0.09	–	2.53(0.14)	5.5	≤0.12	–	0.92(0.24)	5.4	2.89(0.52)	5.0
SO: $14_{14}-13_{13}$	602.292	≤0.12	–	2.25(0.21)	5.1	≤0.16	–	≤0.38	–	2.28(0.69)	4.3
SO: $14_{15}-13_{14}$	603.021	≤0.10	–	2.84(0.13)	5.5	≤0.14	–	≤0.31	–	3.94(0.38)	5.6
SO_2: $5_{51}-4_{40}$	555.666	≤0.26	–	0.77(0.22)	4.1	≤0.18	–	≤0.52	–	≤1.43)	–
SO_2: $15_{610}-15_{511}$	560.891	≤0.10	–	0.49(0.12)	8.3	≤0.11	–	≤0.26	–	0.69(0.33)	3.6
SO_2: $13_{68}-13_{59}$	561.266	≤0.12	–	≤0.13	–	≤0.13	–	≤0.29	–	2.49(0.39)[b]	5.2
SO_2: $11_{66}-11_{57}$	561.491	≤0.10	–	≤0.11	–	≤0.12	–	≤0.25	–	1.02(0.38)	6.1
SO_2: $10_{64}-10_{55}$	561.560	≤0.09	–	≤0.14	–	≤0.11	–	≤0.27)	–	0.86(0.55)	5.0
SO_2: $11_{48}-10_{37}$	567.593	≤0.10	–	0.61(0.10)	4.7	≤0.12	–	≤0.24	–	1.00(0.31)	4.4
SO_2: $6_{51}-5_{42}$	574.807	≤0.07	–	0.72(0.10)	4.2	≤0.11	–	≤0.25	–	1.31(0.26)	5.9
SO_2: $12_{48}-11_{39}$	587.568	≤0.11	–	0.69(0.14)	5.5	≤0.69	–	≤0.37	–	2.15(1.92)	7.0
SO_2: $7_{53}-6_{42}$	593.945	≤0.12	–	0.60(0.12)	3.9	≤0.14	–	≤0.37	–	0.66(0.58)	3.3
SO_2: $13_{410}-12_{39}$	604.367	≤0.07	–	0.88(0.11)	5.9	≤0.12	–	≤0.30	–	1.16(0.34)	4.2
SO_2: $8_{53}-7_{44}$	613.076	≤0.08	–	0.62(0.12)	4.1	≤0.10	–	≤0.19	–	1.33(0.62)	5.9
SO_2: $14_{410}-13_{311}$	626.087	≤0.09	–	0.56(0.15)	4.4	≤0.12	–	≤0.28	–	≤1.14	–
SO_2: $9_{55}-8_{44}$	632.193	≤0.12	–	0.63(0.16)	4.2	≤0.16	–	≤0.26	–	1.63(0.47)	5.1

Notes. The CH_3OH lines detected in at least a source other than NGC 6334I are reported in Table 4. Note that we did not report the list of CH_3OCH_3 lines as they are detected in NGC 6334I only and are the focus of a forthcoming paper. For each source, we report the main beam temperature integrated intensity $T_{\rm mb}\Delta v$ (K km s^{-1}), and the FWHM Δv (km s^{-1}) obtained by fittting the line with a gaussian. In parenthesis we report the rms over the same integration interval of the line intensity. Only lines with rms larger than 3 are considered detected, except in the case of NGC 6334I, where 1σ was taken since the rms is artificially higher because of the line-crowed spectrum. Upper limits refer to 1σ.
[a] Line is heavily absorbed; [b] line is merged; [c] only the central component.

Table 4. List of detected lines of CH_3OH.

Transition	Freq.	L1157-B1		IRAS 16293		OMC2-IRAS 4		AFGL 2591		NGC 6334I	
		$T_{mb}\Delta v$	Δv	$T_{mb}\Delta v$	Δv	$T_{mb}\Delta v$	Δv	$T_{mb}\Delta v$	Δv	$T_{mb}\Delta v$	Δv
	(GHz)	K km s^{-1}	km s^{-1}	K km s^{-1}	km s^{-1}	K km s^{-1}	km s^{-1}	K km s^{-1}	km s^{-1}	K km s^{-1}	km s^{-1}
$11_{20}-10_{10}$	558.345	≤0.13	–	0.49(0.12)	6.3	1.53(0.12)	3.3	≤0.31	–	6.57(1.72)	5.3
$3_{-20}-2_{-10}$	568.566	≤0.10	–	0.85(0.11)	4.0	2.35(0.13)	4.3	≤0.26	–	9.72(0.47)	5.7
$17_{0+0}-16_{1+0}$	568.784	≤0.09	–	≤0.10	–	0.74(0.14)	3.3	≤0.25	–	3.81(0.50)	5.3
$15_{-10}-14_{00}$	572.899	≤0.08	–	≤0.13)	–	1.20(0.09)	3.6	≤0.23	–	4.82(0.52)	5.4
$12_{1+0}-11_{1+0}$	574.868	≤0.09	–	0.41(0.11)	4.7	1.30(0.10)	4.1	0.83(0.22)	9.1	5.96(0.86)	5.5
$12_{0+2}-11_{0+2}$	577.996	≤0.07	–	0.43(0.12)	5.7	1.67(0.12)	3.8	≤0.28	–	5.65(1.15)	5.8
$12_{00}-11_{00}$	578.006	≤0.09	–	0.53(0.11)	6.2	1.61(0.11)	3.7	≤0.29	–	5.48(1.25)	5.6
$2_{2-0}-1_{1-0}$	579.085	0.46(0.08)	6.2	0.76(0.13)	4.5	1.84(0.11)	4.3	≤0.25	–	9.96(4.55)	5.3
$12_{-10}-11_{-10}$	579.150	0.43(0.09)	5.2	0.53(0.14)	4.1	2.84(0.09)	3.5	≤0.26	–	≤6.43	–
$12_{0+0}-11_{0+0}$	579.460	≤0.07	–	0.57(0.14)	5.0	3.01(0.09)	3.7	≤0.26	–	6.98(0.68)	5.5
$12_{2-0}-11_{2-0}$	579.858	≤0.08	–	≤0.12	–	0.62(0.10)	4.1	≤0.35	–	8.14(6.18)	8.2
$2_{2+0}-1_{1+0}$	579.921	≤0.10	–	0.59(0.13)	4.4	1.69(0.09)	4.2	≤0.28	–	13.00(3.60)	8.0
$12_{6+0}-11_{6+0}$	579.933	≤0.09	–	0.81(0.17)	5.7	1.79(0.19)	4.3	≤0.34	–	10.58(3.88)	6.5
$12_{10}-11_{10}$	580.369	≤0.09	–	0.49(0.11)	5.9	1.09(0.12)	3.8	≤0.28	–	6.26(3.06)	5.8
$12_{2+0}-11_{2+0}$	580.502	≤0.08	–	≤0.12	–	0.59(0.13)	4.1	≤0.26	–	5.39(3.35)	5.3
$12_{20}-11_{20}$	580.903	≤0.08	–	0.68(0.12)	6.4	1.47(0.10)	3.6	≤0.27	–	6.25(0.63)	5.4
$12_{-20}-11_{-20}$	581.092	≤0.08	–	0.49(0.13)	6.4	0.84(0.13)	4.3	≤0.20	–	6.34(0.44)	5.9
$6_{1+0}-5_{0+0}$	584.450	0.82(0.10)	6.7	1.31(0.12)	4.1	4.06(0.14)	3.9	≤0.27	–	13.38(0.54)	5.9
$12_{1-0}-11_{1-0}$	584.822	≤0.14	–	0.48(0.15)	6.0	1.78(0.13)	3.7	≤0.34	–	8.56(0.94)	9.2
$23_{-30}-22_{-40}$	587.622	≤0.12	–	3.23(0.16)	4.2	3.45(0.39)	9.4	0.88(0.27)	4.4	16.38(1.23)	7.1
$7_{3+0}-6_{2+0}$	590.278	≤0.13	–	0.76(0.12)	5.8	2.29(0.15)	3.7	≤0.31	–	10.26(0.51)	5.6
$7_{3-0}-6_{2-0}$	590.440	≤0.11	–	0.77(0.15)	4.4	2.19(0.15)	3.7	1.04(0.26)	8.0	9.92(0.62)	5.4
$9_{00}-8_{-10}$	590.791	≤0.13	–	0.70(0.23)	5.6	1.99(0.15)	3.7	≤0.28	–	6.25(1.44)	4.8
$9_{10}-8_{00}$	602.233	≤0.13	–	0.47(0.20)	4.5	1.52(0.19)	3.7	≤0.35	–	7.49(2.56)	5.3
$12_{20}-11_{10}$	607.216	≤0.14	–	≤0.38	–	1.29(0.18)	3.5	≤0.33	–	5.77(0.86)	5.2
$13_{1+0}-12_{1+0}$	622.659	≤0.09	–	0.53(0.12)	7.3	1.22(0.12)	4.0	≤0.27	–	9.57(1.10)	8.2
$13_{00}-12_{00}$	625.749	≤0.10	–	0.38(0.13)	5.5	1.51(0.12)	3.7	≤0.35	–	6.06(0.78)	5.9
$13_{2+1}-12_{2+1}$	626.609	≤0.13	–	0.71(0.22)	3.7	2.14(0.39)	4.3	≤0.36	–	11.46(2.90)	6.5
$3_{2-0}-2_{1-0}$	626.626	≤0.10	–	0.59(0.14)	3.4	2.22(0.12)	4.5	≤0.31	–	9.80(2.84)	5.6
$13_{01}-12_{01}$	626.640	≤0.11	–	0.63(0.16)	3.5	2.18(0.33)	4.4	≤0.38	–	8.78(2.31)	5.1
$13_{-10}-12_{-10}$	627.170	≤0.09	–	0.75(0.14)	6.5	2.70(0.13)	3.9	≤0.29	–	5.20(1.38)	4.6
$13_{1-2}-12_{1-2}$	627.187	≤0.11	–	0.68(0.21)	6.7	3.32(0.96)	4.6	≤0.33	–	5.72(1.95)	4.9
$13_{0+0}-12_{0+0}$	627.558	≤0.11	–	0.65(0.14)	5.5	2.72(0.11)	3.8	≤0.29	–	6.90(1.00)	5.4
$13_{a10}-12_{a10}$	627.572	≤0.11	–	0.71(0.15)	6.6	2.86(0.33)	3.9	≤0.31	–	6.99(1.18)	5.5
$14_{-60}-15_{-50}$	628.042	≤0.09	–	≤0.12	–	0.61(0.13)	4.7	≤0.27	–	8.97(2.97)	9.2
$13_{2-0}-12_{2-0}$	628.052	≤0.10	–	≤0.17	–	0.62(0.14)	4.7	≤0.30	–	9.22(2.95)	9.4
$13_{3+0}-12_{3+0}$	628.470	≤0.09	–	≤0.20	–	0.68(0.24)	4.8	≤0.30	–	≤5.22	–
$13_{4-0}-12_{4-0}$	628.512	≤0.10	–	≤0.18	–	1.30(0.27)	10.2	≤0.30	–	≤3.60	–
$13_{3-0}-12_{3-0}$	628.525	≤0.09	–	≤0.10	–	1.31(0.11)	10.0	≤0.31	–	13.23(4.49)	11.1
$13_{10}-12_{10}$	628.696	≤0.14	–	0.43(0.18)	6.9	1.00(0.12)	3.9	≤0.31	–	4.35(0.88)	4.3
$13_{30}-12_{30}$	628.816	≤0.10	–	0.49(0.12)	7.6	0.42(0.11)	6.0	≤0.34	–	5.54(3.80)	5.6
$13_{2+0}-12_{2+0}$	628.869	≤0.10	–	≤0.12	–	0.58(0.11)	4.5	≤0.30	–	5.76(3.61)	5.3
$3_{2+0}-2_{1+0}$	629.140	0.51(0.11)	6.3	0.86(0.15)	4.2	2.06(0.14)	4.0	≤0.34	–	12.61(0.61)	5.8
$13_{20}-12_{20}$	629.322	≤0.12	–	0.48(0.15)	6.0	1.42(0.11)	3.9	≤0.33	–	6.34(1.45)	5.4
$13_{-20}-12_{-20}$	629.652	≤0.09	–	≤0.14	–	0.76(0.12)	4.4	≤0.28	–	6.22(0.60)	5.4
$7_{1+0}-6_{1+0}$	629.921	0.51(0.12)	5.8	1.29(0.11)	4.3	4.22(0.10)	3.9	≤0.26	–	13.51(0.50)	6.1
$13_{1-0}-12_{1-0}$	633.423	≤0.11	–	0.46(0.16)	5.7	1.69(0.14)	3.7	≤0.38	–	6.45(0.57)	5.2

Notes. Only lines detected in at least a source other than NGC 6334I are reported. Columns are as in Table 3. Note that the nomenclature for the transition is the one from the JPL catalog.